Clin Pharmacokinet 2002; 41 (8): 581-602
0312-5963/02/0008-0581/$25.00/0



# Pharmacokinetic Imaging

## A Noninvasive Method for Determining Drug Distribution and Action

*Alan J. Fischman,*[1,2] *Nathaniel M. Alpert*[1] and *Robert H. Rubin*[1,2]

1 Division of Nuclear Medicine of the Department of Radiology, Massachusetts General Hospital and Harvard Medical School, Boston, Massachusetts, USA

2 Division of Health Sciences and Technology, Center for Experimental Pharmacology and Therapeutics, Harvard-Massachusetts Institute of Technology, Cambridge, Massachusetts, USA

## Contents



## Abstract

Advances in positron emission tomography (PET), single photon emission computed tomography (SPECT) and magnetic resonance spectroscopy (MRS), and the ability to label a wide variety of compounds for *in vivo* use in humans, have created a new technology for making precise physiological and pharmacological measurements. Due to the noninvasive nature of these approaches, repetitive and/or continuous measurements have become possible. Thus far, these techniques have been primarily used for one-time assessments of individuals. However, experience suggests that a major use of this technology will be in the evaluation of new drug therapies. Already, these techniques have been used to measure precisely and noninvasively the pharmacokinetics of a variety of antimicrobial, antineoplastic and CNS agents. In the case of CNS drugs, imaging

techniques (particularly PET) have been used to define the classes of neuroreceptors with which the drug interacts. The physiological, pharmacological and biochemical measurements that can be performed noninvasively using modern imaging techniques can greatly facilitate the evaluation of new therapies. These measurements are most likely to be useful during drug development in preclinical studies and in phase I/II human studies. Preclinically, new drugs can be precisely compared with standard therapies, or a series of analogues can be screened for further development on the basis of performance in animal models. In Phase I/II, imaging measurements can be combined with classical pharmacokinetic data to establish optimal administration schedules, evaluate the utility of interventions in specific clinical situations, and aid in the design of Phase III trials.

In recent years, the techniques employed for drug discovery, design and evaluation have undergone many changes. Historically, the process of drug discovery involved screening of large numbers of samples of natural products for biological effects until a compound with the desired properties was identified. After elucidation of the structure of this potential drug, large numbers of analogues were prepared by standard methods of organic chemistry and screened with *in vitro* and *in vivo* assays until an agent or agents with optimal pharmacology emerged. Lead compounds from this discovery and design process were further evaluated to define their pharmacokinetic and pharmacodynamic profiles by studies of normal animals and animal models of the condition for which the drug was being developed. Tissue distribution studies in large numbers of animals yielded precise pharmacokinetic data, and detailed physiological monitoring produced information about pharmacodynamics. Candidate drugs that continued to show promise in the animal studies were further evaluated in Phase I to III studies in humans. Compared with the results of animal studies, data obtained from human clinical trials were less extensive. In general, the quality of blood and plasma pharmacokinetic data obtained from human subjects were comparable to those from animal studies; however, information about tissue distribution was considerably less precise and usually limited to body secretions and biopsy samples. Similarly, pharmacodynamic evaluations were much less extensive.

Drug discovery, design and evaluation are currently performed with a much higher degree of sophistication. In contrast to the largely empirical procedures of the past, modern drug development is usually directed to specific molecular targets and is guided by principles of molecular structure and dynamics, genomics and proteomics. Laborious one-by one synthesis and biological evaluation of analogues has been supplemented by approaches based on combinatorial chemistry and high-throughput screening methods. Applications of genetic engineering to drug design (gene therapy) has fostered a transition from developing drugs for treating symptoms to the design of agents that correct or modulate pathophysiology of disease processes.

Recent developments in techniques for noninvasive imaging of drug distribution and effect have begun to have similar impact on drug evaluation in humans. In numerous situations, imaging procedures such as positron emission tomography (PET), single photon emission computed tomography (SPECT) and magnetic resonance spectroscopy (MRS) can provide tissue pharmacokinetic information in humans that is comparable in detail and quality to the results from invasive studies in animals. With PET, it has been possible to obtain detailed quantitative information about drug pharmacokinetics and pharmacodynamics in a variety of tissues, including the CNS. This review will concentrate on recent applications of PET to pharmacokinetic analysis. Although SPECT and MRS are less generally applicable to pharmacokinetic analysis, several important applications of these approaches will also be discussed.

## 1. Radionuclide Imaging Techniques

### 1.1 Instrumentation

Radionuclide imaging techniques have the goal of providing noninvasive measurements of the three-dimensional distribution of radiolabelled compounds in living organisms.[1] In many aspects, radionuclide imaging is similar to conventional serial section autoradiography. However, instead of film, an array of scintillation detectors is used to record images.

Three different procedures are currently used for radionuclide imaging: planar imaging, SPECT and PET. The technical details of the three techniques vary considerably, however, the general principles are similar.

With planar imaging, a large sodium iodide scintillation detector optically coupled to an array of photomultiplier tubes is placed close to the object of interest and emitted photons are measured (figure 1).[1] By appropriate interconnections of the photomultiplier tubes, two-dimensional projections of the distribution of radioactivity in the object are obtained. By acquiring images in multiple projections, three-dimensional distribution of radioactivity can be estimated. The instrumentation for SPECT is similar to that used for planar imaging; however, projections at all angles around an axis of the object are acquired. These data are then reconstructed using filtered back-projection or iterative algorithms (similar to x-ray computed tomography) to produce transaxial, coronal and sagittal images of the distribution of radioactivity.

Imprecise quantification is the major disadvantage of both planar and SPECT imaging. This deficiency is caused by loss of photons by tissue attenuation and by imprecise positioning of disintegrations due to scatter within the body. Furthermore, obtaining a γ- camera image requires absorptive collimation of photons emitted by the radioactive object.[1] These collimators are made of lead and contain many parallel-aligned channels that allow detection of only those photons that pass through the channels from the source to the crystal.

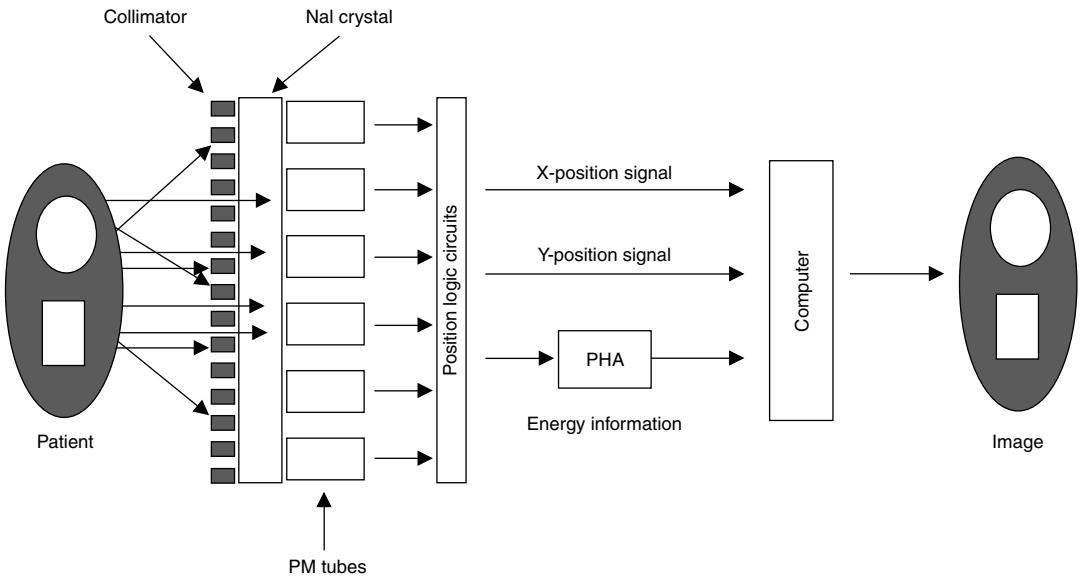


**Fig. 1.** Basic components of a single photon imaging device (Anger camera) used for planar or single photon emission computed tomography (SPECT) imaging. **PHA** = pulse height analyser; **PM** = photomultiplier.

Photons that travel in other orientations are absorbed by the collimator (figure 1) and do not contribute to the image. This method of collimation imposes significant limits on both detection sensitivity and image resolution.

The main problems inherent to single photon imaging are not important issues with PET. Many radionuclides with low atomic number and relative proton excess decay by emission of positrons (positive electrons, $\beta^+$).[2] After a positron is emitted, it rapidly loses kinetic energy and eventually combines with an electron ($\beta^-$). $\beta^+$-$\beta^-$ interaction results in an annihilation event in which the rest mass of the positron-electron pair is converted to energy. The relationship $E = mc^2$ predicts that this process will result in two 511 KeV photons emitted in opposite directions. In PET imaging devices, these photons are recorded by detector pairs oriented at 180° to each other (figure 2). The use of appropriate electronics, coincidence circuitry, ensures that only those photon pairs that occur in a very short time interval (5 to 20 nsec) and are the result of individual $\beta^+$-$\beta^-$ annihilations are recorded. This process of annihilation, coincidence and detection defines a volume between the detectors from which coincidence events originate (figure 2).[3] By positioning rings of detectors around the object, maps of the three-dimensional distribution of positron emitting isotope in an object can be reconstructed using filtered-back projection or iterative algorithms. The process of annihilation, coincidence and detection is frequently referred to as 'electronic collimation' and is the primary reason why the sensitivity of PET is 10- to 20-fold higher than that of SPECT. Since corrections for attenuation and scatter are straightforward with PET, the images are quantitative and precise maps of radiopharmaceutical distribution.[2] Furthermore, since resolution is limited only by positron range and detector characteristics, PET images have higher resolution than SPECT images, 1 to 6mm versus 7 to 18mm full width at half maximum (FWHM).

### 1.2 Tracer Techniques

Noninvasive measurement of the tissue pharmacokinetics of a drug requires radiolabelling with

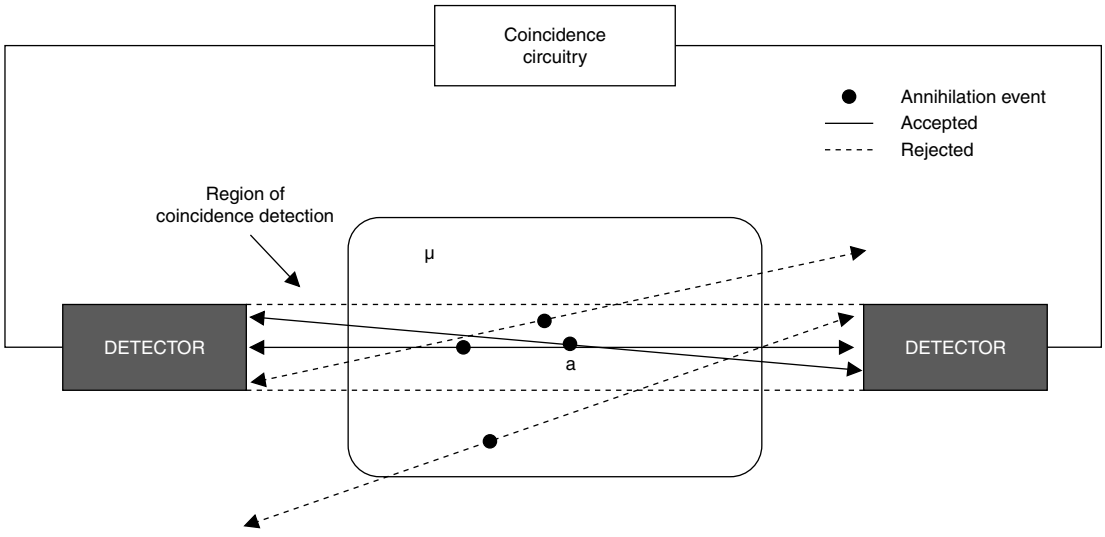


**Fig. 2.** Basic principles of annihilation-coincidence-detection. For an event to be recorded, both photons have to arrive at opposing detectors within the resolving time of the coincidence circuitry. Events registered by a single detector are rejected, giving 'electronic collimation'.

an isotope that emits penetrating radiation that can be detected by external imaging. A critical requirement of the radiolabelling process is that it must not modify the biological or biochemical properties of the drug.[4] Usually, this requires radiolabelling of the compound under investigation with a radioactive form of one of the atoms that is present in its native structure: carbon, hydrogen, nitrogen or oxygen. Drugs labelled with $^{14}C$ and/or $^{3}H$ have been of great value for studying pharmacokinetics in animals; however, the negative electrons that are emitted in their radioactive decay have a range of only a few millimetres and thus cannot be detected outside the human body. The only radioactive forms of carbon, oxygen and nitrogen with emissions that can be detected externally are positron emitters. Also, many drugs contain one or more fluorine atoms in their native structure and can be radiolabelled with the positron emitter $^{18}F$. Because there are no isotopes of hydrogen that are suitable for external imaging, positron emitting halogen isotopes are frequently substituted for hydrogen of hydroxyl groups. These analogues are not guaranteed to retain the pharmacokinetic properties of the native drug; however, the substitutions are highly conservative and in many situations have yielded useful probes. Several common positron emitting radionuclides that have been used in PET studies are listed in table I.

### 1.3 Radiochemistry

The products of most nuclear reactions that are currently used for preparing PET radionuclides are relatively simple molecules, such as $^{13}NH_3$, $^{11}CO_2$, $H^{18}F$ or $^{18}F_2$. In many situations, incorporating these building blocks into complex drugs is straightforward chemically; however, the short half-lives of most PET radionuclides introduce complications.[4] Radiopharmaceutical synthesis must be sufficiently rapid so that the drug of interest can be synthesised, isolated, purified and formulated as a sterile, pyrogen-free, isotonic solution within 2 to 3 half-lives of the radionuclide. Also, since large amounts of radioactivity must be handled, limitation of exposure to personnel is an important consideration. For most drugs, these issues require the design and synthesis of drug precursors that can be radiolabelled in a single step. Over the past several years, these requirements have fostered the development of many new methods of rapid remote-controlled and robotics-based chemistry.

### 1.4 Advantages and Limitations of Positron Emission Tomography Measurements

Compared with conventional methods of pharmacokinetic analysis and other noninvasive techniques, PET has many clear and important advantages. (i) PET is noninvasive, requiring at most arterial blood sampling. (ii) Extremely high sensitivity permits measurements at drug concentrations as low as $10^{-12}$ mol/L (based on detection sensitivity of 1 nCi/cm$^3$ and a drug labelled at a specific activity of 1000 mCi/μmol). (iii) The availability of positron emitting radionuclides of nitrogen, carbon and fluorine makes it possible to prepare a PET tracer for almost any drug. (iv) Due to the quantitative nature of PET measurements, drug concentrations in tissue determined by imaging are nearly identical to the results of direct measurements of radioactivity in samples of excised tissue (figure 3). (v) The anatomical resolu-

**Table I.** Physical characteristics of radionuclides used for positron emission tomography

| Radionuclide | Half-life (min) | Target reaction | Common forms |
|---|---|---|---|
| $^{15}O$ | 2.0 | $^{14}N$ (d,n) $^{15}O$ | $^{15}O_2$, $C^{15}O_2$, $C^{15}O$ |
| $^{13}N$ | 10.0 | $^{16}O$ (p,α) $^{13}N$ | $^{13}NH_3$, $^{13}N_2$ |
| $^{11}C$ | 20.4 | $^{14}N$ (p,α) $^{11}C$ | $^{11}CO_2$, $^{11}CO$, $^{11}CH_3I$ |
| $^{18}F$ | 110 | $^{18}O$ (p,n) $^{18}F$ | $^{18}F_2$, $H^{18}F$ |
| $^{76}Br$ | 972 | $^{75}As$ ($^{3}He$,2n) $^{76}Br$ | $^{76}Br_2$ |
| $^{124}I$ | 6048 | $^{124}Te$ (d,2n) $^{124}I$; $^{124}Te$ (p,n) $^{124}I$ | $Na^{124}I$ |

tion of PET permits measurements in small volumes of tissue. (vi) The extremely high biochemical resolution of PET allows differentiation of physiological alterations that occur nanometres apart. For example, PET images of patients with Parkinson's disease (figure 4) demonstrate reduced presynaptic dopamine metabolism (imaged with [$^{18}$F]fluorodopa) and normal expression of postsynaptic $D_2$ receptors (imaged with [$^{11}$C]-raclopride). (vii) The short physical half-lives of most PET tracers results in favourable radiation dosimetry that allows repetitive measurements in a single subject after physiological or pharmacological interventions. (viii) Due to the high specific activities of most PET tracers, physiological and pharmacological effects are negligible. (ix) Most importantly, after suitable toxicity studies and with rigorous process control procedures, PET radiopharmaceuticals developed for studies in animals can be applied to investigations in healthy volunteers and patients. Since PET tracers are chemically and biologically identical to the native unlabelled drug, only limited toxicity studies are required.

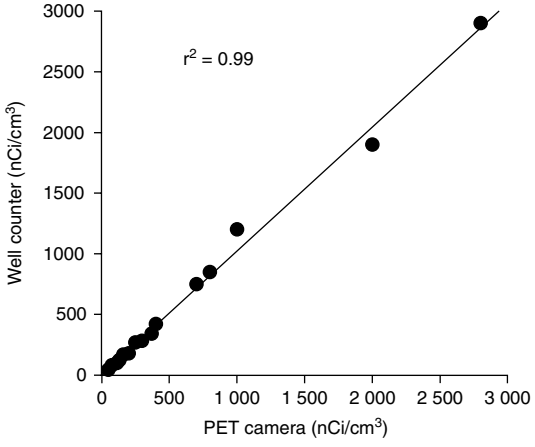


**Fig. 3.** Relationship between drug concentrations determined by positron emission tomography (PET) and direct 'well-counter' measurements of excised tissue samples.[5] As indicated, the points fall nearly along the line of identity.

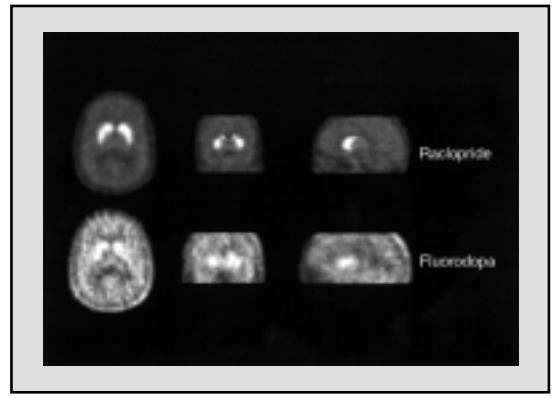


**Fig. 4.** Positron emission tomography transaxial, coronal and sagittal images of a patient with Parkinson's disease demonstrating reduced presynaptic dopamine metabolism (imaged with [$^{18}$F]fluorodopa) and normal expression of postsynaptic $D_2$ receptors (imaged with [$^{11}$C]raclopride).

The short physical half-lives of most PET tracers present several complications for pharmacokinetic studies. (i) Most radioactive drugs must be prepared separately for each subject by a cyclotron/radiochemistry facility that is in close proximity to the imaging laboratory. (ii) The time interval over which pharmacokinetic studies can be performed is limited. In general, this time frame is approximately four times the physical half-life of the tracer; approximately 40 min with $^{13}$N, 80 min with $^{11}$C and 8 hours with $^{18}$F. Obviously, this is less of a problem with $^{76}$Br- and $^{124}$I-labelled tracers. (iii) The number of chemical manipulations that can be employed for preparing PET radiopharmaceuticals is limited. (iv) Since only total radioactivity in tissue is measurable by PET, quantification is accurate only if metabolism is minimal. (v) Although the anatomical resolution of PET is far superior to that of all other radionuclide methods, it is much lower than that of computed tomography, MRI or ultrasound.

## 2. Types of Studies with Positron Emission Tomography

From the perspective of PET studies of tissue pharmacokinetics, most therapeutic agents can be

classified into one of two broad categories. The first class of drugs includes pharmaceuticals that interact with and/or neutralise agents that invade the organism from the environment (toxins, bacteria, fungi and viruses) or alter normal physiological function from within (neoplastic cells). Important examples of these types of drugs are antimicrobial and antineoplastic agents (table II). Members of the second group of drugs target specific biomolecules and modulate disease-associated alterations of cellular processes or homeostatic control systems. Examples of these drugs include antipsychotics, steroids, nonsteroidal anti-inflammatory agents, enzyme inhibitors and biologically active proteins and peptides.

In general, the type of pharmacokinetic information that is desired is different for the two classes of drugs and the PET techniques required for the measurements vary considerably. For the first type of agents, only tissue concentrations of drug are usually required. For these studies, the drug is labelled with a positron emitter, injected into volunteers or patients and serial PET images are acquired. These images are quantitative maps of the concentration of radioactivity ($nCi/cm^3$) in tissue. If the tracer is not metabolised in the tissues of interest, dividing each pixel in the images by the specific activity of the tracer (nCi/μmol) produces a map of regional concentrations of intact drug. By constructing regions of interest (ROIs) on the images, the time dependence of drug concentrations in specific organs and tissues can be determined and used to calculate standard pharmacokinetic parameters such as peak concentrations, plateau concentrations and areas under concentration-time curves.

The situation is much different for the second class of agents. These drugs usually elicit their therapeutic effects by interacting with specific receptors or binding molecules, and PET studies focus on the derivation of values for receptor number ($B_{max}$) and affinity ($K_D$). These investigations require high specific activity radiolabelling, arterial blood sampling, measurement of metabolite concentrations in the circulation and detailed kinetic modelling of the results of single or multiple injection studies (see section 2.2).

In the following sections, we will describe the results of PET studies of the pharmacokinetics of both types of drugs. Antimicrobial agents and drugs that affect the CNS will be used as examples of the first and second types of drugs.

### 2.1 Antimicrobial Agents

To be effective, antimicrobial therapy must deliver concentrations of active drug to the site of infection that are sufficient to inhibit growth of, or kill, the invading microorganism. Drug concentra-

**Table II.** Examples of type 1 drugs that have been studied by positron emission tomography

| Drug | Radiolabel | Class | Reference |
|---|---|---|---|
| Cisplatin | $^{13}N$ | Antineoplastic | 6 |
| Carmustine (BCNU) | $^{11}C$ | Antineoplastic | 7 |
| SarCNU | $^{11}C$ | Antineoplastic | 7 |
| Elmustine (HECNU) | $^{11}C$ | Antineoplastic | 8 |
| Fluorotamoxifen | $^{18}F$ | Antineoplastic | 9 |
| SN-22995 (DACA) | $^{11}C$ | Antineoplastic | 10 |
| Temozolomide | $^{11}C$ | Antineoplastic | 11 |
| Fluorouracil | $^{18}F$ | Antineoplastic | 12 |
| Erythromycin | $^{11}C$ | Antifungal | 13 |
| Fluconazole | $^{18}F$ | Antimicrobial | 14 |
| Fleroxacin | $^{18}F$ | Antimicrobial | 15 |
| Lomefloxacin | $^{18}F$ | Antimicrobial | 16 |
| Trovafloxacin | $^{18}F$ | Antimicrobial | 17 |

**DACA** = [(dimethylamino)ethyl]acridine-4-carboxamide; **SarCNU** = 2-chloroethyl-3-sarcosinamide-1-nitrosourea.

tions can be measured serially in blood and urine; however, other body fluids and most tissues are not easily sampled in humans. Thus, in designing clinical trials in patients with infection, administration schedules are usually based on tissue pharmacokinetic studies in animals and on human blood and urine data. Unfortunately, there is frequently an imprecise relationship between drug concentrations in blood and urine and concentrations achieved in tissues such as brain, liver and prostate. Clearly, approaches in which traditional blood and urine measurements can be correlated with tissue concentrations determined by PET hold great promise for defining appropriate dosage schedules and in accelerating drug development.

#### 2.1.1 Erythromycin

Erythromycin was the first antimicrobial agent for which tissue pharmacokinetic measurements were made with PET. In these studies, *N*-demethyl-erythromycin was radiolabelled with [$^{11}$C]formaldehyde by reductive methylation[13] to yield a product that was chromatographically identical to authentic erythromycin.

After intravenous injection of this radiopharmaceutical, the time course of drug accumulation was measured by PET in normal and infected lung of patients with pneumonia.[18] During the first hour after injection, extravascular concentration of drug was similar in normal and infected tissue ($6.6 \pm 2.2$ *vs* $5.5 \pm 2.2$ μg/g). These concentrations were achieved within 10 min after radiopharmaceutical administration and remained relatively constant for 60 min.

This study was successful for two reasons. First, the presence of an *N*-methyl group in the native structure of erythromycin and the availability of *N*-demethyl-erythromycin resulted in a simple and straightforward (single-step) method for radiolabelling. Secondly, the rapid equilibration of erythromycin in pulmonary tissue made the 20 min physical half-life of $^{11}$C appropriate for labelling – the tracer and the process were well matched. Unfortunately, precursors for radiolabelling most antimicrobial agents are less readily available and, for many agents, tissue equilibration is much slower. This requires the preparation of new precursors and radiolabelling with longer lived radionuclides for meaningful measurements.

#### 2.1.2 Fluconazole

Fluconazole is a fungistatic agent[19-21] that elicits its effects by inhibiting fungal cytochrome P450 sterol C-14 α-demethylation, which results in depletion of normal fungal sterols and accumulation of 14α-methyl sterols.[22-25] The combination of broad spectrum fungistatic action, low systemic toxicity[26] and a favourable pharmacokinetic profile make this drug an attractive therapeutic agent. Use of fluconazole in the treatment of invasive fungal infections caused by organisms such as *Cryptococcus neoformans*, *Candida* species, *Coccidioides immitis*, *Histoplasma capsulatum* and *Blastomyces dermatitidis* has been a major advance in antimicrobial chemotherapy.[27] However, use of fluconazole as the primary treatment for disseminated cryptococcal infection in AIDS patients and in the primary treatment of acute life-threatening fungal infections in immunocompromised hosts has remained somewhat controversial.[28] Important aspects of this controversy have been questions about optimal dosage schedules and actual concentrations of drug achieved in different tissues, particularly sites of infection. Although tissue distribution of fluconazole has been measured in laboratory animals[29,30] and concentrations in body fluids were measured in humans,[31-35] detailed studies of tissue distribution and concentrations in humans were lacking.

The presence of two fluorine atoms in the native structure of fluconazole made it an ideal candidate for $^{18}$F radiolabelling and PET studies. Also, because fluconazole undergoes minimal metabolism *in vivo*, measurements of tissue and blood radioactivity accurately reflect concentrations of intact drug.[29,30,34] Unfortunately, the method for commercial preparation of fluconazole introduces both fluorine atoms at an early stage of the synthesis and thus is not applicable for producing $^{18}$F-labelled drug. To overcome this problem, a new fluconazole precursor into which $^{18}$F can be introduced in a single synthetic step was synthesised. This pro-

cedure yielded pharmaceutical grade [$^{18}$F]fluconazole that was identical chemically and in terms of antimicrobial activity to the usually prescribed drug.[15]

In preliminary studies, this radiopharmaceutical was used to measure the pharmacokinetics of fluconazole by PET in normal rabbits and rabbits with candidal infections.[5] When $^{18}$F-labelled drug was coinjected with a pharmacological dose of unlabelled drug, there was rapid equilibration to a relatively uniform distribution in most organs of the rabbit. In contrast, when [$^{18}$F]fluconazole was injected 'carrier-free', blood clearance was accelerated, spleen, muscle and heart accumulation was decreased and liver accumulation was increased. These results illustrate the importance of using clinically relevant doses of drug for PET pharmacokinetic studies.

In subsequent studies, [$^{18}$F]fluconazole was used to measure tissue pharmacokinetics in healthy volunteers by PET.[36] Figure 5 illustrates representative PET images of brain, heart, lung, liver, spleen, kidney and skeletal muscle of human subjects at 90 min after injection of [$^{18}$F]fluconazole plus unlabelled fluconazole (5 mg/kg). These images demonstrate significant accumulation of fluconazole in all organs studied. When injected with a pharmacological dose of unlabelled drug, [$^{18}$F]-fluconazole accumulates to a significant extent in all of the peripheral organs of humans. In contrast with the results obtained in rabbits, the pattern of fluconazole accumulation is much less homogeneous in humans. Fluconazole concentrations ranged from a low of $1.24 \pm 0.27$ μg/g in bone to a high of $22.96 \pm 0.24$ μg/g in spleen; values in the other tissues studied exceeded 6 μg/g. These concentrations compare well with the concentrations required to inhibit the growth of a variety of pathogens *in vitro*. Thus, the PET data indicate that the usual fluconazole dose of 5 mg/kg should be effective for treatment of hepatosplenic and urinary tract candidal infection and maintaining remission of cryptococcal meningitis in AIDS patients. However, the clinical efficacy of fluconazole might be improved by increasing the dose for conditions such as fungal osteomyelitis or the primary treatment of acutely life-threatening CNS and intravascular infections. In the case of CNS infections, increasing the dosage of drug based on the results of the PET measurements resulted in a marked improvement in efficacy (unpublished results).

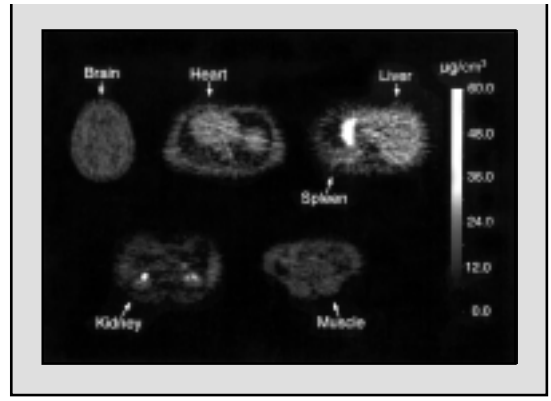


**Fig. 5.** Representative positron emission tomography images of healthy human volunteers co-injected with [$^{18}$F]fluconazole plus unlabelled fluconazole 5 mg/kg. The grey scale is calibrated in terms of absolute concentration (μg/cm$^3$).[36]

#### *2.1.3 Fluoroquinolones*

In recent years, fluoroquinolone antimicrobial agents have achieved an important role in the treatment of a variety of bacterial infections. Since these agents contain one or more fluorine atoms, $^{18}$F-labelled drugs are useful for PET measurements of *in vivo* pharmacokinetics. Studies with fleroxacin represent the first application of PET to this class of drugs.[37-40] These studies followed similar lines to the measurements with [$^{18}$F]fluconazole; a specific precursor was synthesised and a rapid method for $^{18}$F labelling was devised. This was followed by PET studies in normal animals, animals with bacterial infection, and humans. As with fluconazole, these studies provided important new information about tissue pharmacokinetics in animal models and humans.

Although these types of measurements would be useful for many other fluoroquinolones, the re-

quirement of a specific precursor for each drug is a major limitation. Fortunately, this problem has been largely resolved by the observation that the fluoroquinolone lomefloxacin can be radiolabelled by $^{18}F$ for $^{19}F$ exchange.[16] Recently, this approach was applied to the preparation of $^{18}F$-labelled trovafloxacin.[17]

### 2.2 CNS Drugs

Measurements of the tissue pharmacokinetics of drugs that act in the CNS vary considerably in approach and complexity. These studies can be broadly divided into two types: direct and indirect. For direct studies, the drug is radiolabelled with a positron emitter and dynamic imaging is performed. If drug distribution is the only information that is required, the studies are performed by the methods described for evaluation of antimicrobial agents. In contrast, when the goal is to derive specific values for the parameters of drug-receptor interaction, imaging protocols are much more complex. In the case of drugs that bind to a single class of receptors, time-activity curves from single or multiple injection studies can be analysed by compartmental modelling to estimate receptor density ($B_{max}$), binding affinity ($K_D$) or binding potential ($B_{max}/K_D$). When the drug is expected to interact with multiple receptors, kinetic parameters for a specific receptor type can be measured by blocking the other receptors with unlabelled ligands with which they interact. For example, *N*-methylspiperone binds to both dopamine $D_2$ and serotonin 5-$HT_2$ receptors; however, parameters for binding to 5-$HT_2$ receptors can be estimated from PET studies in which $D_2$ receptors are blocked with haloperidol.

In indirect studies, the receptor binding profile of the drug of interest is derived from coinjection or displacement studies with radiolabelled test ligands that bind to specific receptors. One of the most important examples of this approach was the evaluation of the dopamine $D_2$ and $D_1$ receptor binding characteristics of the atypical antipsychotic clozapine using [$^{11}C$]raclopride and [$^{11}C$]-SCH-23390 as test ligands for $D_2$ and $D_1$.[41-44] Receptor types that have been studied by this method include dopaminergic, serotonergic, cholinergic, opioid and benzodiazepine binding sites. Table III lists some of the PET ligands that are currently available for this type of study.

A variety of kinetic models have been used for estimating parameters of ligand-receptor interaction by PET.[59,64-67] All of these models include transport of free ligand from blood to tissue and receptor binding. Binding may be reversible or irreversible, and a nonspecific binding compartment may or may not be required. Figure 6 illustrates one of the most general models for ligand transport and binding. In this configuration, flux of ligand across the blood-brain barrier, $K_1$, is equal to $p \bullet V_r \bullet Ca(t)$, where p is the permeability, $V_r$ is the fraction of brain tissue available for ligand-receptor interaction and Ca(t) is the metabolite-corrected concentration of radioactivity in plasma. Free ligand, F, can either bind directly to an unoccupied receptor, a nonspecific site (NS, $k_5$) or escape from the tissue ($k_2$). The probability for ligand-receptor interaction depends on the rate constant for association ($k_{on}$) and the local concentration of unoccupied receptors ($B'_{max}$). The rate constants for dissociation of specific and nonspecific binding are $k_{off}$ and $k_6$. Because even high specific activity ligands contain significant amounts of unlabelled drug, which can affect local concentrations of unoccupied receptors, kinetics of unlabelled ligand must also be modelled. Thus, this general model for ligand-receptor interaction contains two components with the same structure and parameters. The differential equations defined by the model can be solved by nonlinear least squares, to yield estimates of the kinetic parameters.

With this model, seven parameters must be identified from imaging data. However, the PET time-activity curves acquired after injection of a radioligand are relatively simple; a rapidly rising phase, a plateau and a falling phase. When these data are analysed with the model depicted in figure 7, the number of parameters to be fitted is too large to yield meaningful results. Fortunately, in some cases, this problem can be resolved by multiple

**Table III.** Examples of radioligands that have been used for positron emission tomography imaging

| Receptor | Ligand | Specificity | References |
|---|---|---|---|
| Dopamine | [$^{11}$C]SCH-23390 | $D_1$ | 41,42 |
| | [$^{11}$C]SCH-39166 | $D_1$ | 45 |
| | [$^{11}$C]Methylspiperone | $D_2$, $5HT_2$ | 46 |
| | [$^{76}$Br]Bromospiperone | $D_2$, $5HT_2$ | 47 |
| | [$^{11}$C]Raclopride | $D_2$ | 41,42 |
| | [$^{76}$Br]Bromolisuride | $D_2$ | 48 |
| | [$^{11}$C]CFT | Transporter | 49 |
| | [$^{11}$C]Altropane | Transporter | 50 |
| Serotonin | [$^{18}$F]Setoperone | $5HT_2$ | 51 |
| | [$^{11}$C]MBL | $5HT_2$ | 52 |
| | [$^{11}$C]WAY-100635 | $5HT_{1A}$ | 53 |
| Benzodiazepine | [$^{11}$C]Flumazenil | $BZ_1$, $BZ_2$ | 54 |
| | [$^{11}$C]PK-11195 | 'Peripheral' | 55 |
| Opioid | [$^{11}$C]Carafentanyl | μ | 56 |
| | [$^{11}$C]Diprenorphine | μ, κ | 57 |
| | [$^{18}$F]Acetylcyclofoxy | μ | 58 |
| Acetylcholine (muscarinic) | [$^{11}$C]MQNB | $M_1$, $M_2$ | 59 |
| | [$^{11}$C]Levetimide | $M_1$, $M_2$ | 60 |
| | [$^{11}$C]Scopolamine | $M_1$, $M_2$ | 61 |
| | [$^{11}$C]Cogentin | $M_1$, $M_2$ | 62 |
| Adrenergic | [$^{11}$C]CGP-12177 | $\beta_1$, $\beta_2$ | 63 |

**CFT** = 2β-carbomethoxy-3β-aryltropane; **MBL** = *N*$^1$-methyl-2-bromo-lysergic acid diethylamide; **MQNB** = methylquinuclidinyl benzilate.

injection imaging protocols, which results in much more detailed time-activity curves. An example of the application of this approach was use of $^{11}$C-labelled 2β-carbomethoxy-3β-aryltropane ([$^{11}$C]-CFT) to determine the kinetics of dopamine transporter sites using a three-injection protocol.[68] At the beginning of the study, high specific activity radioligand was injected and PET data were collected for 30 min. An excess of unlabelled CFT plus a small amount of [$^{11}$C]CFT was then injected and data collection was continued for 60 min. At 90 min, a second injection of high specific activity radioligand was administered and imaging was continued for 30 min. Figure 7 illustrates a representative time-activity curve for [$^{11}$C]CFT in monkey striatum measured using this protocol. The fitted curve and the time dependence of the concentration of radioactivity in each compartment are also indicated. Values for $K_D$ and $B'_{max}$ estimated by this approach were in excellent agreement with the results of *in vitro* assay. Modifications of this approach have been used for modelling CNS kinetics of [$^{11}$C]flumazenil and [$^{76}$Br]-bromolisuride.[54,67]

In some situations, simpler procedures have yielded useful information. For measuring dopamine $D_2$ receptor density with 3-(2′-[$^{18}$F]-fluoroethyl)spiperone, only two injections (tracer and displacement) were required.[69] With ligands that dissociate rapidly from their receptors, equilibrium binding is established and an even simpler approach has been employed.[70,71] In this situation, regional time-activity curves are used to establish a time that represents equilibrium of specific binding. A series of PET scans are then performed at varying specific activity, and $K_D$ and $B'_{max}$ are calculated from saturation curves or Scatchard plots.[72]

Although these complex multi-injection protocols are required for precise estimates of individual values of $K_D$ and $B'_{max}$, the ratio of these parameters, referred to as binding potential ($B'_{max}/K_D$ [73]) can be determined from single injection studies. Fortunately, in many situations important informa-

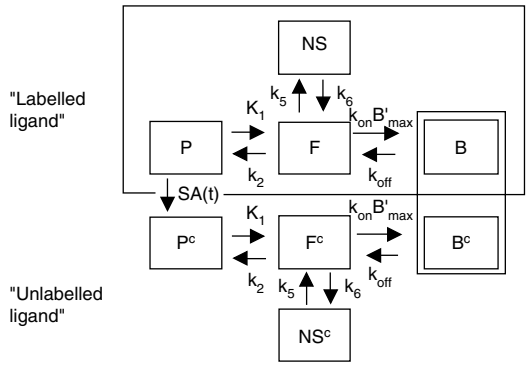


**Fig. 6.** Model for ligand transport and binding. This formulation illustrates the interaction of labelled and unlabelled ligand. Although unlabelled ligand concentrations are not directly measurable by positron emission tomography, the concentration of specifically bound unlabelled ligand affects the local concentration of free receptors and thus binding of labelled ligand. **B** = bound ligand in tissue; $\mathbf{B'}_{max}$ = local concentration of unoccupied receptors; **F** = free ligand in tissue; $\mathbf{k}_{on}$ = rate constant for specific binding; $\mathbf{k}_{off}$ = rate constant for dissociation of specific binding; $\mathbf{K}_1$ = rate constant for flux of ligand into tissue; $\mathbf{k}_2$ = rate constant for escape from tissue; $\mathbf{k}_5$ = rate constant for nonspecific binding; $\mathbf{k}_6$ = rate constant for dissociation of nonspecific binding; **NS** = nonspecifically bound ligand; **P** = free ligand in plasma; **SA(t)** = specific activity at time t.

tion can be obtained from measurements of binding potential. For example, one of the most common questions in drug development is the degree to which a new drug affects occupancy (%ΔRO) of a class of receptors (equation 1):

$$\%\Delta RO = \frac{RO_{Bl} - RO_{Drug}}{RO_{Bl}} \times 100 = \frac{B'_{max} - B''_{max}}{B'_{max}} \times 100$$

where $RO_{Bl}$ = receptor occupancy before drug treatment, $RO_{Drug}$ = receptor occupancy after drug treatment, $B'_{max}$ = concentration of available receptors before drug treatment, and $B''_{max}$ = concentration of available receptors after drug treatment. Since it can be assumed that $K_D$ is unaffected by drug treatment, changes in binding potential reflect changes in $B'_{max}$ and (equation 2):

$$\%\Delta RO = \frac{BP_{Bl} - BP_{Drug}}{BP_{Bl}} \times 100$$

where $BP_{Bl}$ = binding potential before drug treatment and $BP_{Drug}$ = binding potential after drug treatment. This type of analysis was used to study central 5-$HT_2$ receptor occupancy of an antipsychotic drug, ziprasidone, in healthy volunteers at various times after administration.[74] In this investigation, dynamic PET studies with the $5HT_2$ receptor ligand [$^{18}$F]setoperone were performed in healthy volunteers, in the drug-naive state and at 4, 8, 12 and 18 hours after a single oral dose of ziprasidone. Quantification of cortical binding potential was performed by a modification of the method described by Petit-Taboue et al.[75] Individual values for the parameters $K_1$, $k_2$, $k_5$ and $k_6$ were estimated by fitting the three-compartment model shown in figure 8 to cerebellar time-activity curves. To determine binding potential, the parameters $K_1/k_2$, $k_5$ and $k_6$ were fixed at the cerebellar values, $V_b$ was fixed at 4.5% and $K_1$, $k_3$ and $k_4$ were estimated by fitting the cortical time-activity curves to the four-compartment model shown in figure 8. Binding potential was calculated from the individual values of $k_3$ and $k_4$.

As expected, the images demonstrate high concentrations of [$^{18}$F]setoperone in the cerebral cortex at baseline. In images acquired at 4 hours after administration of ziprasidone, there was a marked decrease in cortical accumulation of radioactivity and concentrations were only slightly greater than cerebellar activity. In the images acquired at 8, 12 and 18 hours after ziprasidone, intermediate levels of cortical radioactivity were observed. Figure 9 shows the effect of time after administration on receptor occupancy. Since it can be assumed that $K_D$ is unaffected by drug treatment, %RO reflects changes in $B'_{max}$. These data indicate that there is >95% receptor occupancy at 4 hours after administration, and that occupancy remains above 50% for more than 19 hours. These findings clearly establish that once daily administration should be adequate with this drug. Also, as indicated in figure 9, the relationship between receptor occupancy and blood concentrations of drug is quite imprecise.

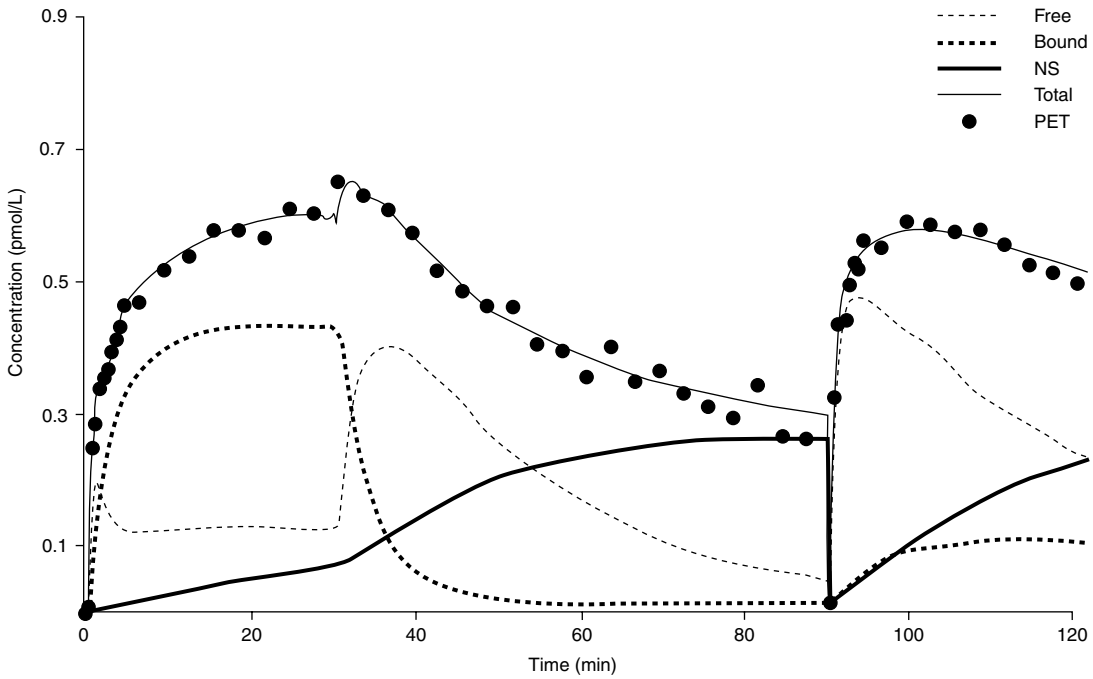


**Fig. 7.** Typical least-squares fit of a positron emission tomography (PET) time-activity curve for the average concentration of $^{11}$C-labelled 2β-carbomethoxy-3β-aryltropane in monkey striatum based on the kinetic model in figure 6 and the injection protocol outlined in the text. The time-dependence of the model estimates of concentrations of radioactivity in free, specifically bound and nonspecifically bound (NS) compartments is also illustrated.[68]

In another investigation, this type of analysis was used to study the potential novel antidepressant BMS-181101.[76] This drug was believed to influence CNS serotonin neurotransmission by several different mechanisms and thus differs from specific serotonin reuptake inhibitors, such as fluoxetine, paroxetine and fluvoxamine. BMS-181101 is a potent inhibitor of serotonin reuptake by the terminal bouton *in vitro*, thereby potentiating the synaptic actions of serotonin. In addition, it acts as a full agonist at dorsal raphe somatodentritic 5-$HT_{1A}$ autoreceptors and presynaptic terminal 5-$HT_{1D}$ receptors that regulate the activity of serotonin neurons. To study its pharmacokinetics and receptor binding in the brains of healthy volunteers, $^{11}$C-labelled BMS-181101 was prepared by methylation with $^{11}CH_3I$ at the 5-methoxy position of the piperazine ring, and dynamic PET imaging was performed in six volunteers. Two studies were performed in each subject. For the first study, the subjects were injected with 10 mCi of high specific activity [$^{11}$C]BMS-181101 (~4000 mCi/μmol) and serial PET images and arterial blood samples were collected over 90 min. At 30 min after acquiring the final image, each subject was co-injected with a second dose of 10 mCi of [$^{11}$C]BMS-181101 plus 3.9mg of unlabelled drug (final specific activity ~1.5 mCi/μmol) and imaging and blood collection were repeated. The data were analysed by calculating regional tracer accumulation (% injected dose/g) at 60 min after injection and compartmental modelling. Metabolite-corrected arterial input functions were used in the calculations and the vascular fraction of brain tissue ($V_b$) was fixed at 4%. Measurements of % injected dose/g yielded similar values

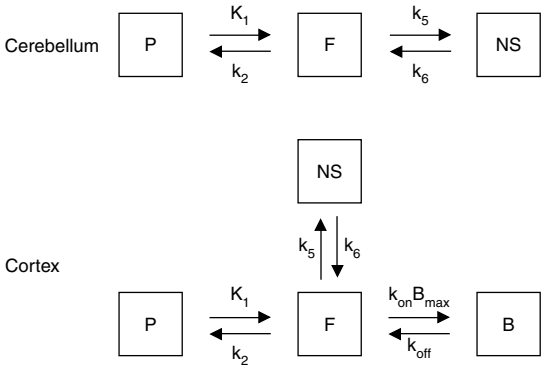


**Fig. 8.** Compartmental models describing the kinetics of [$^{18}$F]setoperone in human brain. Three- and four-compartment models were used to analyse cerebellar and cortical time-activity curves respectively. **B** = bound ligand in tissue; $\mathbf{B_{max}}$ = local concentration of unoccupied receptors; **F** = free ligand in tissue; $\mathbf{k_{on}}$ = rate constant for specific binding; $\mathbf{k_{off}}$ = rate constant for dissociation of specific binding; $\mathbf{K_1}$ = rate constant for flux of ligand into tissue; $\mathbf{k_2}$ = rate constant for escape from tissue; $\mathbf{k_5}$ = rate constant for nonspecific binding; $\mathbf{k_6}$ = rate constant for dissociation of nonspecific binding; **NS** = nonspecifically bound ligand; **P** = free ligand in plasma.

for all brain regions, independent of specific activity. Kinetic modelling of time activity curves for cerebellum, caudate, putamen, thalamus, pons and temporal, occipital and frontal cortex demonstrated that tissue distribution could be described by a simple two-compartment flow model. Statistical comparisons of the apparent distribution volumes for each region failed to reveal significant differences between the high and low specific activity studies.

This study clearly demonstrates the usefulness of PET in drug development. Although *in vitro* studies of the interaction of BMS-181101 with a variety of serotonin receptor systems demonstrated significant binding, this was not observed *in vivo*. In fact, the results of the PET study in conjunction with equivocal results of phase II clinical trials resulted in discontinuation of the clinical evaluation of BMS-181101. Clearly, PET studies at an earlier phase of drug development (late Phase I) might have resulted in considerable savings of time, money and other resources.

In some situations data analysis can be further simplified by the use of graphical methods. The first application of this technique was described by Patlak et al.[77] for radioligands that bind irreversibly to their receptors ($k_4 \approx 0$) on the imaging time scale and free ligand is in steady state with the blood. In this analysis, the ratio of tissue to plasma radioactivity is plotted versus 'normalised time' (integral of plasma radioactivity from time 0 to t divided by plasma radioactivity at time t). The asymptotic slope and intercept of the linear part of this curve yields estimates of binding potential. Subsequently, Logan et al.[78] extended this approach to reversible systems. Although estimates of binding potential calculated by these methods are sometimes less precise than the results of kinetic modelling, the techniques can be used to produce parametric images that represent pixel by pixel maps of binding potential. Figure 10 illustrates binding potential images of the brain of a healthy volunteer at baseline and 4 hours after administration of ziprasidone.

## 3. Pharmacodynamics

In addition to their value for noninvasive *in vivo* studies of pharmacokinetics, radionuclide tech-

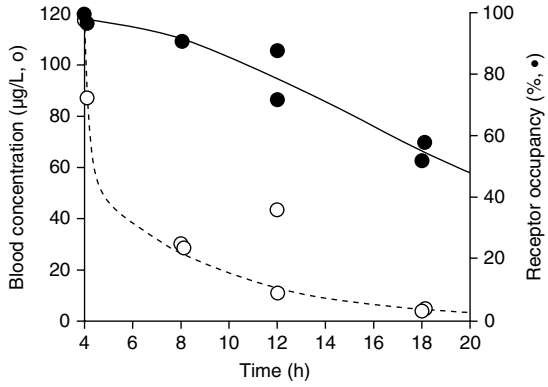


**Fig. 9.** Effect of time after administration of [$^{18}$F]setoperone on serotonin $5HT_2$ receptor occupancy determined by least-squares fitting of positron emission tomography data to the model illustrated in figure 8. The time dependence of blood concentrations of drug is also illustrated.[74]

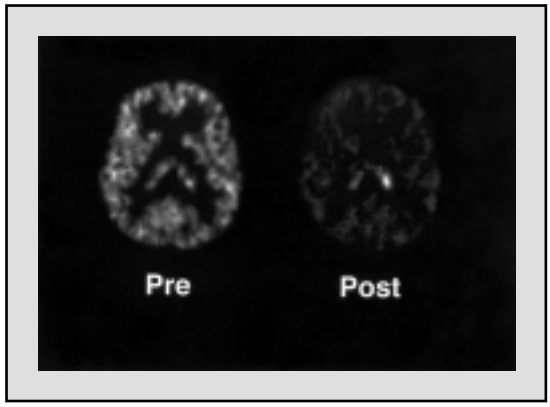


**Fig. 10.** Representative parametric images of the brain of a healthy volunteer illustrating the distribution of binding potential before (left) and 4 hours after (right) oral administration of ziprasidone.[74]

niques also have considerable utility for assessing drug effects at the organ, tissue and cellular level, i.e. pharmacodynamic studies. Although PET measurements have superior sensitivity and quantitative reliability for these measurements, many types of pharmacodynamic studies can also be performed with SPECT or planar imaging. The limited sensitivity and the difficulty of labelling compounds without changing their pharmacological properties are major obstacles to the application of SPECT in drug development; however, these factors are less severe restrictions for pharmacodynamic studies. Two important advantages of SPECT are: (i) because of the variety of energies of photons emitted by SPECT radiopharmaceuticals, multiple tracers can be studied simultaneously; and (ii) SPECT facilities are available in almost every nuclear medicine department.

Since nearly every PET or SPECT radiopharmaceutical can serve as a 'biomarker' for pharmacodynamic studies, exhaustive evaluation of this topic would require discussion of a vast array of imaging procedures, a task that is clearly beyond the scope of this review. Specific examples of PET and SPECT radiopharmaceuticals that can be applied for pharmacodynamic studies are summarised in table IV, and several examples of these procedures are discussed in the remainder of this section.

In a recent study, the utility of $^{99m}$Tc-tetrofosmin ($^{99m}$Tc-TF) and thallium-201 ($^{201}$TlCl) for predicting multidrug resistance (MDR) and radioresistance was investigated in patients with lung cancer.[79] Thirty patients with untreated disease underwent dual isotope SPECT at 10 and 120 min after co-injection of the radiopharmaceuticals, and retention of each tracer was evaluated semiquantitatively both at baseline and after sequential (n = 12) or concurrent (n = 18) radiation and chemotherapy (cisplatin plus etoposide). In patients treated with sequential therapy, the response to radiation was predicted by $^{99m}$Tc-TF retention, whereas $^{201}$Tl retention was found not to be predictive. Regardless of whether the sequential or concurrent protocol was applied, 14/18 tumours with high $^{99m}$Tc-TF retention (≥15%) exhibited a favourable response to chemoradiotherapy, whereas all 12 tumours with low $^{99m}$Tc-TF retention (≤15%) did not respond to the therapy.

The *in vivo* potency of euphorigenic doses of intravenous cocaine for displacing binding of 2β-carbomethoxy-3β-(4-[$^{123}$I]iodophenyl)tropane-([$^{123}$I]β-CIT) binding to striatal dopamine transporters (DAT) was assessed in human cocaine abusers by SPECT.[80] In this investigation, cocaine abusers (n = 6) were injected with [$^{123}$I]β-CIT and imaged 24 hours later under equilibrium conditions. Sequential cocaine infusions (0.28 ± 0.03 and 0.56 ± 0.07 mg/kg) produced significant ($p < 0.0005$) reductions in DAT binding potential. Regression analysis of the logit transformed data enabled reliable determination of the Hill coefficient (0.51) and 50% displacement ($ED_{50}$) dose of cocaine (2.8 mg/kg). These results suggest that cocaine produces behavioural effects in humans at measurable levels of DAT occupancy. In a similar study, the *in vivo* potency of mazindol for binding to DAT was assessed by SPECT with [$^{123}$I]β-CIT.[81] Cocaine-dependent individuals underwent three SPECT scans before, during and after medium-term (1 week) administration of mazindol at

**Table IV.** Examples of radiopharmaceuticals for pharmacodynamic studies by positron emission tomography (PET) and single photon emission computed tomography (SPECT)

| Measurement | SPECT tracers | PET tracers |
|---|---|---|
| Brain perfusion | $^{99m}$Tc-HMPAO | $^{15}CO_2$ |
| | $^{99m}$Tc-ECD | $H_2{}^{15}O$ |
| | | [$^{11}$C] or [$^{15}$O]Butanol |
| | | $^{62}$Cu-PTSM |
| Brain permeability | $^{99m}$Tc-DTPA | $^{68}$Ga-EDTA |
| Blood pool | $^{99m}$Tc-RBCs | $^{11}$CO |
| | $^{99m}$Tc-albumin | $C^{15}O$ |
| | | [$^{11}$C]Albumin |
| Bone function | $^{99m}$Tc-MDP | $^{18}F^-$ |
| Hepatobiliary function | $^{99m}$Tc-DISIDA | $^{68}$Ga-HBED |
| Infection | $^{111}$In- or $^{99m}$Tc-WBCs | $^{18}$F- or $^{11}$C-labelled peptides |
| Reticuloendothelial system function | $^{99m}$Tc-colloid | [$^{18}$F]FDG |
| | | $^{68}$Ga-colloids |
| Lung function | $^{133}$Xe/$^{99m}$Tc-MAA | $C^{18}O_2$ |
| | | $^{13}N_2$ |
| Myocardial perfusion | $^{201}$Tl | $^{13}NH_3$ |
| | $^{99m}$Tc-isonitriles | $H_2{}^{15}O$ |
| | $^{99m}$Tc-teboroxime | $^{82}$Rb |
| | | [$^{15}$O]Butanol |
| | | $^{62}$Cu-PTSM |
| Glomerular filtration rate | $^{99m}$Tc-DTPA | $^{68}$Ga-EDTA |
| | $^{123}$I-iothalamate | |
| Renal perfusion | $^{99m}$Tc-MAG3 | $H_2{}^{15}O$ |
| | | $^{82}$Rb |
| Thyroid function | $^{123}I^-$ | $^{124}I^-$ |
| | $^{99m}$Tc-pertechnetate | |
| Tumours | $^{67}$Ga-citrate | [$^{18}$F]FDG |
| | $^{99m}$Tc-MIBI | [$^{11}$C]Methionine |
| | $^{99m}$Tc- tetrofosmin | [$^{11}$C]Leucine |
| | $^{123}$I-MIBG | [$^{11}$C]Thymidine |
| | $^{111}$In-octreotide | $^{124}$I-MIBG |
| | | $^{18}$F-estradiol |
| Glucose metabolism | | [$^{18}$F]FDG |
| Glucose transport | | [$^{11}$C]3-*O*-Methyl-glucose |
| Protein synthesis | $^{77}$Se-Methionine | [$^{11}$C]Methionine [$^{11}$C]Leucine |
| DNA synthesis | | [$^{11}$C]Thymidine |
| | | $^{18}$F-FLT |
| Energy metabolism | $^{123}$I-fatty acid analogues | $^{15}O_2$ |
| | | [$^{11}$C]Acetate |
| | | [$^{11}$C]Fatty acids |

**DISIDA** = di-isopropyl iminodiacetic acid; **DTPA** = diethylenetriaminepenta-acetic acid; **ECD** = ethylcysteinate dimer; **EDTA** = ethylenediamine-*N,N,N′,N′*-tetra-acetic acid; **FDG** = fluorodeoxyglucose; **FLT** = 3'-deoxy-3'flurothymidine; **HBED** = *N,N′*-bis(2-hydroxybenzyl)-ethylenediamine-*N,N′*-diacetic acid; **HMPAO** = hexamethylpropylene amine oxime; **MAA** = macroaggregated albumin; **MAG3** = mercaptoacetyltriglycine; **MDP** = methylene diphosphonate; **MIBG** = *m*-iodobenzylguanidine; **MIBI** = methoxy isobutyl isonitrile; **PTSM** = pyruvaldehyde-bis($N^4$-methylthiosemicarbazone); **RBC** = red blood cell; **WBC** = white blood cell.

doses of 2 and 4 mg/day. For each scan, subjects were injected with [$^{123}$I]β-CIT and imaged 24 hours later under equilibrium conditions. These measurements demonstrated a significant effect of mazindol dose ($p < 0.001$) on reducing DAT binding potential. Regression analysis of the logit transformed data enabled estimation of the $ED_{50}$ of mazindol (30 mg/day). These data suggest that low doses of mazindol occupy a small percentage (<25%) of DAT in human cocaine abusers and that much higher, potentially intolerable, doses (≥30 mg/day) may be required to significantly antagonise cocaine binding *in vivo*.

## 4. Magnetic Resonance Spectroscopy

Conventional magnetic resonance imaging (MRI) employs magnetic field gradients to produce images of the distribution and relaxation properties of nuclei with magnetic spins. Since individual atoms of all drugs have specific resonance frequencies, in principle it should be possible to record MR images of any drug or drug metabolite. Unfortunately, due to the intrinsic insensitivity of magnet resonance detection, MRI has largely been limited to images of the distribution and spin properties of water (tissue concentration about 55 mol/L). Because of this sensitivity limitation, in most applications of MRS images are not recorded. Instead, field gradients are used to select a specific region of tissue and record a spectrum. Even with this approach, sensitivity is much lower than with PET, $10^{-5}$ to $10^{-3}$ mol/L[82] compared with about $10^{-12}$ mol/L.

Despite this low sensitivity, MRS has much to offer in specific areas of pharmacokinetic analysis. First, although PET can provide precise measurements of total drug concentrations present in small volumes of tissue, MRS can be used to determine the contributions of different molecular species present. Also, differentiation between intra- and extracellular drug may be possible. Secondly, as with PET, the number of tracers that are available for MRS studies is potentially unlimited. Although the majority of MRS studies have been performed with drugs that contain fluorine ($^{19}$F) in their native structure, isotopes with non-zero spin are available for all atoms in drugs, for example $^{1}$H, $^{13}$C, $^{15}$N, $^{17}$O and $^{31}$P. For MRS, $^{19}$F has the advantages of high intrinsic sensitivity, a large range of chemical shifts and zero natural background. $^{1}$H also has high sensitivity; however, the range of chemical shifts is much smaller and natural background is high. $^{13}$C and $^{15}$N have much lower intrinsic sensitivities, but they can be useful for MRS studies when advanced pulse sequences are employed. Thirdly, in contrast to PET tracers, drugs for MRS studies are stable compounds with unlimited shelf lives and there is no potential danger from exposure to ionising radiation. Although MRS exposes humans to radiofrequency energy and strong magnetic fields, studies with conventional imaging systems have not been associated with significant health risks.[83] Finally, the time interval over which pharmacokinetic studies can be performed is unlimited with MRS – matching the half-life of the tracer to the time scale of the process under investigation is not an issue.

In the following sections, applications of MRS to studies of antineoplastic drugs and antimicrobial agents, and of drugs that affect the CNS, will be discussed as examples of the first and second types of drugs previously described in section 2.

### 4.1 Antineoplastic Drugs

Although numerous antineoplastic agents have been evaluated by MRS (table V), the most extensive clinical experience has been gained by $^{19}$F-MRS studies of the pharmacokinetics of fluorouracil (5- FU).[84] This drug, and several of its metabolites, have been measured *in vivo* in animals and patients using standard clinical MR systems. For 5-FU, tumoral half-life is the parameter that can be measured most readily. This parameter is of importance because trapping of 5-FU in tumours is a necessary, albeit not a sufficient, condition for response. Patients in whom tumoral half-life of 5-FU is ≥20 min are designated as 'trappers', whereas individuals with lower values are 'non-trappers'. In a study of 75 patients with liver metastases from colorectal carcinoma,[85] 49% of

**Table V.** Examples of antineoplastic agents that have been studied by magnetic resonance spectroscopy

| Drug | Signal | Measurement | References |
|---|---|---|---|
| Fluorouracil | $^{19}F$ | Pharmacokinetics | 84,85 |
| Gemcitabine | $^{19}F$ | Distribution and metabolism | 86 |
| Difluorochlorambucil | $^{19}F$ | Tumour hypoxia | 87 |
| SR-4554 | $^{19}F$ | Tumour hypoxia | 88 |
| Iproplatin | $^{1}H$ | Early distribution | 89 |
| Ifosfamide | $^{31}P$ | Pharmacokinetics | 90 |
| Temozolomide | $^{13}C$ | Pharmacokinetics | 91 |
| Carboplatin | $^{195}Pt$ | Distribution | 92 |
| Tirapazamine | $^{31}P$ (phosphates) | Tumour energy metabolism | 93 |
| Chemotherapy/radiation | $^{1}H$ | Lactate concentration | 94 |

37 patients with tumoral half-life of ≥20 min responded to the drug, whereas 51% did not. In contrast, the 38 patients with tumoral half-life shorter than 20 min did not respond. These findings suggest that $^{19}F$-MRS may become a useful screening procedure for withdrawing 5-FU treatment in non-trappers. In other investigations, the effects of modulators and other agents on tumoral half-life of 5-FU have been measured by MRS. These $^{19}F$-MRS studies have been extended to other fluoropyrimidines, some of which are prodrugs of 5-FU, and others where the fluorine atom is on the ribose ring.

### 4.2 Antimicrobial Agents

The *in vivo* pharmacokinetics of fleroxacin has been measured in human liver and muscle by $^{19}F$-MRS.[95] This study demonstrated a pharmacokinetic pattern similar to the results of PET studies. However, due to the much lower intrinsic sensitivity of MRS, spatial resolution was quite low, the measurements were restricted to large volumes of tissue, and absolute quantification was difficult. Nevertheless, this study clearly pointed out the potential of studies in which PET and MRS measurements are combined. PET can provide precise measurements of total drug concentrations present in small volumes of tissue, whereas MRS can be used to determine contributions of different molecular species present (intact drug *vs* metabolites) and possibly to differentiate between intra- and extracellular drug. In the case of fleroxacin, in which >90% of the drug is in the intact form, such a combination approach is probably not necessary. However, for drugs that undergo a greater degree of metabolism, such complex analysis could be of considerable value.

### 4.3 CNS Drugs

Due to the low sensitivity of the technique, most MRS studies of CNS active drugs have concentrated on measurements of whole-brain pharmacokinetics. However, despite this limitation, a considerable amount of important information has been obtained. One of the earliest investigations in this area used $^{7}Li$-MRS to measure brain lithium concentrations in healthy volunteers after single and multiple doses of lithium carbonate.[96] The results of this study demonstrated that relatively slow accumulation of lithium in the brain may be responsible for the delay in therapeutic response that is frequently observed after initiation of therapy. In a later MRS study, an unexpected variability in brain versus serum concentrations of lithium was demonstrated in patients with bipolar disease.[97]

Several investigations have employed $^{19}F$-MRS to measure brain concentrations of psychiatric drugs. In one study, the technique was used to measure concentrations of fluoxetine and norfluoxetine in patients with obsessive compulsive disorder and major depression.[98] This study demonstrated that the brain to plasma ratio of the parent drug (plus metabolite) was significantly elevated to 2.6,

which may have implications for understanding both the therapeutic and the toxic effects of fluoxetine. In another study, brain concentrations of paroxetine or fluoxetine were measured before and after 3 days of placebo substitution in patients with remitted major depression who were taking 20 mg/day of either drug.[99] With placebo substitution, a mean of 88% of brain fluorine signal from fluoxetine (plus metabolites) remained, compared with a mean of 38% of the brain fluorine signal from paroxetine (plus metabolites). In patients initially taking paroxetine, adverse events during placebo substitution were highly correlated with steady-state drug concentrations in the brain.

In another study, $^{19}$F-MRS was used to quantify brain concentrations of dexfenfluramine in humans receiving clinical doses of the drug and to determine whether human brain dexfenfluramine concentrations approach those reported to cause irreversible neurochemical changes in animals.[82] Twelve obese women received dexfenfluramine 15mg twice daily for 90 days; $^{19}$F-MRS measurements were performed at baseline and three times during treatment. Brain concentrations of dexfenfluramine and its active metabolite dexnorfenfluramine reached steady state (about 4 μmol/L) in the brain after approximately 10 days of treatment and did not increase significantly during the remainder of the treatment period. These findings demonstrated that fluorinated drugs can be quantified by $^{19}$F-MRS at concentrations below 10 μmol/L in the human brain. The time course data suggested that brain dexfenfluramine concentrations parallel plasma pharmacokinetics. Also, brain dexfenfluramine/dexnorfenfluramine concentrations were well below those previously found to cause irreversible brain alterations in animals.

These results clearly indicate that MRS has a bright future for pharmacokinetic analysis. Although MRS will never have the sensitivity of PET, as higher field magnet systems become more widely available and improved pulse sequences are developed, sensitivity will improve considerably and a greater variety of drugs will become appropriate for study.

## 5. Conclusions

Physiological and biochemical measurements that can be performed noninvasively in humans using modern imaging techniques can greatly facilitate the evaluation of new therapies. Two critical points in drug development where these measurements are likely to be most useful are in preclinical studies and in Phase I/II studies. In preclinical studies, a new drug can be precisely compared with standard therapies, or a series of analogues can be screened for further development on the basis of performance in appropriate animal models. In Phase I/II human studies, classical pharmacokinetic measurements can be combined with imaging measurements to define optimal administration schedules and the potential utility of interventions in particular clinical situations, and to design Phase III studies that are crucial for drug licensure. In general, the types of measurements that are possible can be grouped into the following categories.

(i) In those situations in which the drug can be radiolabelled, the time course of tissue delivery can be determined noninvasively *in vivo* in health and disease. Such information should be most useful for determining administration schedules, establishing efficacy and predicting possible toxicity.

(ii) Ligand-receptor binding can be assessed *in vivo* in two ways. The ability of the drug to displace standard radiolabelled ligands from their receptors can be determined or, alternatively, labelled drug can be used to more directly assess distribution and time course of binding. These measurements are of particular value for studying drugs that act on the central nervous and cardiovascular systems.

(iii) Measurements of tissue metabolism will be useful in determining the effects of therapies aimed at particular metabolic abnormalities. These measurements may also be useful in defining the viability and function of tissues in such widely disparate clinical situations as cancer chemotherapy and cardiology.

We would suggest that the coupling of classical clinical pharmacology with imaging-based measurements will help form the basis for future drug development.

## Acknowledgements

Studies from our laboratory that were presented in this review were supported in part by grants from Bristol-Myers Squibb Inc., Pfizer Inc., and the US Public Health Service.

## References

1. Sorenson JA, Phelps ME. Physics in nuclear medicine. The Anger camera: basic principles. 2nd ed. New York: Grune & Stratton, Inc, 1987: 298-317
2. Hoffman EJ, Phelps ME. Positron emission tomography: principles and quantitation. In: Phelps ME, Massiotta JC, Schelbert MR, editors. Positron emission tomography and autoradiography. New York: Raven Press, 1986: 237-86
3. Phelps ME, Hoffman EJ, Mullani NA, et al. Application of annihilation coincidence detection to transaxial reconstruction tomography. J Nucl Med 1975; 16: 210-24
4. Fowler JS, Wold AP. Positron emitter-labeled compounds: priorities and problems. In: Phelps ME, Massiotta JC, Schelbert HR, editors. Positron emission tomography and autoradiography. New York: Raven Press, 1986: 391-450
5. Fischman AJ, Alpert NM, Livni E, et al. Pharmacokinetics of 18F-labeled fluconazole in rabbits with candidal infections studied with positron emission tomography. J Pharmacol Exp Ther 1991; 259: 1351-9
6. Ginos JZ, Cooper AJ, Dhawan V, et al. [13N]cisplatin PET to assess pharmacokinetics of intra-arterial versus intravenous chemotherapy for malignant brain tumors. J Nucl Med 1987; 28: 1844-52
7. Mitsuki S, Diksic M, Conway T, et al. Pharmacokinetics of 11C-labelled BCNU and SarCNU in gliomas studied by PET. J Neurooncol 1991; 10: 47-55
8. Conway T, Diksic M. PET studies of potential chemotherapeutic agents: X. Synthesis of "no-carrier-added" (11C)-HECNU: the hydroxyethyl analog of the chemotherapeutic agent BCNU. Int J Rad Appl Instrum [A] 1991; 42: 441-6
9. Inoue T, Kim EE, Wallace S, et al. Preliminary study of cardiac accumulation of F-18 fluorotamoxifen in patients with breast cancer. Clin Imaging 1997; 21: 332-6
10. Brady F, Luthra SK, Brown G, et al. Carbon-11 labelling of the antitumour agent N-[2- (dimethylamino)ethyl]acridine-4-carboxamide (DACA) and determination of plasma metabolites in man. Appl Radiat Isot 1997; 48: 487-92
11. Meikle SR, Matthews JC, Brock CS, et al. Pharmacokinetic assessment of novel anti-cancer drugs using spectral analysis and positron emission tomography: a feasibility study. Cancer Chemother Pharmacol 1998; 42: 183-93
12. Saleem A, Aboagye EO, Price PM. In vivo monitoring of drugs using radiotracer techniques. Adv Drug Deliv Rev 2000; 41: 21-39
13. Pike VW, Palmer AJ, Horlock PL, et al. Semi-automated preparation of a 11C-labelled antibiotic--[N-methyl-11C]erythromycin A lactobionate. Int J Appl Radiat Isot 1984; 35 (2): 103-9
14. Livni E, Fischman AJ, Ray S, et al. Synthesis of 18F-labeled fluconazole and positron emission tomography in rabbits. Int J Appl Radiat Isot Part B 1992; 19: 191-9
15. Livni E, Babich J, Alpert NM, et al. Synthesis and biodistribution of 18F-labeled fleroxacin. Nucl Med Biol 1993; 20: 81-7
16. Tewson TJ. Synthesis of fluorine-18 lomefloxacin, a fluorinated quinolone antibiotic. J Labeled Compds Radiopharm 1993; 32: 145-6
17. Babich JW, Rubin RH, Vincent J, et al. 18F-Labeling and biodistribution of the novel fluoroquinolone antimicrobial agent, trovafloxacin (CP-99,214). Nucl Med Biol 1996; 23: 995-8
18. Wollmer P, Rhodes CG, Pike VW, et al. Measurement of pulmonary erythromycin concentration in patients with lobar pneumonia by means of positron emission tomography. Lancet 1982; II: 1361-4
19. Richardson K, Cooper K, Marriott MS, et al. Design and synthesis of a systemically active agent, fluconazole. Ann N Y Acad Sci 1988; 544: 4-11
20. Richardson K. The discovery and profile of fluconazole. J Chemother 1990; 2: 51-4
21. Richardson K, Cooper K, Tarbit MH, et al. Discovery of fluconazole, a novel antifungal agent. Rev Infect Dis Supp 1990; 3: 267-71
22. Van Den Bossche H, Willemsens G, Cools W, et al. In vitro and in vivo effects of the antimycotic drug ketoconazole on sterol synthesis. Antimicrob Agents Chemother 1980; 17: 922-8
23. Van Den Bossche H, Willemsens G, Cools W, et al. Hypothesis on the molecular basis of the antifungal activities of N-substituted imidazoles and triazoles. Biochem Soc Trans 1983; 11: 665-7
24. Van Den Bossche H. Biochemical targets for antifungal azole-derivative: hypothesis of the mode of action. Curr Top Med Mycol 1985; 1: 313-51
25. Watson PF, Rose ME, Ellis SW, et al. Defective sterol C5-6 desaturation and azole resistance: a new hypothesis for the mode of action of azole antifungals. Biochem Biophys Res Commun 1989; 164: 1170-5
26. Van Cauteren H, Lampo A, Vandenberghe J, et al. Toxicological profile and safety evaluation of antifungal azole derivatives. Mycoses 1989; 32 Suppl. 1: 60-6
27. Saag MS, Dismukes WE. Azole antifungal agents: emphasis on new triazoles. Antimicrob Agents Chemother 1988; 32: 1-8
28. Larsen RA, Leal MA, Chan LS. Fluconazole compared with amphotericin B plus flucytosine for cryptococcal meningitis in AIDS: a randomized trial. Ann Intern Med 1990; 113: 183-7
29. Humphrey MJ, Jevons S, Tarbit MH. Pharmacokinetic evaluation of UK-49,858, a metabolically stable triazole antifungal drug, in animals and humans. Antimicrob Agents Chemother 1985; 28: 648-53
30. Walsh TJ, Foulds G, Pizzo PA. Pharmacokinetics and tissue penetration of fluconazole in rabbits. Antimicrob Agents Chemother 1989; 33: 467-9
31. Brammer KW, Farrow PR, Faulkner JK. Pharmacokinetics and tissue penetration of fluconazole in humans. Rev Infect Dis 1990; 12 Suppl. 3: 318-26
32. Debruyne D, Ryckelynck JP, Bigot MC, et al. Determination of fluconazole in biological fluids by capillary column gas chromatography with a nitrogen detector. J Pharm Sci 1988; 77: 534-5
33. Ebden P, Neill P, Farrow PR. Sputum levels of fluconazole in humans. Antimicrob Agents Chemother 1989; 33: 963-4

34. Foulds G, Brennan DR, Wajszczuk C, et al. Fluconazole penetration into cerebral spinal fluid. J Clin Pharmacol 1988; 28: 363-6
35. Foulds G, Wajszczuk C, Weidler DJ, et al. Steady state parenteral kinetics of fluconazole in man. Ann N Y Acad Sci 1988; 544: 427-30
36. Fischman AJ, Alpert NM, Livni E, et al. Pharmacokinetics of 18F-labeled fluconazole in normal human subjects studied with positron emission tomography. Antimicrob Agents Chemother 1993; 37: 1270-7
37. Livni E, Babich J, Alpert NM, et al. Synthesis and biodistribution of 18F-labeled fleroxacin. Nucl Med Biol 1993; 20: 81-7
38. Fischman AJ, Livni E, Babich J, et al. Pharmacokinetics of 18F-labeled fleroxacin in rabbits with E. coli infections studied with positron emission tomography. Antimicrob Agents Chemother 1992; 36: 2286-92
39. Fischman AJ, Livni E, Babich J, et al. Pharmacokinetics of [18F]fleroxacin in normal human subjects studied with positron emission tomography. Antimicrob Agents Chemother 1993; 37: 2144-52
40. Fischman AJ, Livni E, Babich JW, et al. Pharmacokinetics of [18F] fleroxacin in patients with acute exacerbations of chronic bronchitis and complicated urinary tract infection studied with positron emission tomography. Antimicrob Agents Chemother 1996; 40: 659-64
41. Farde L, Halldin C, Stone-Elander S, et al. PET analysis of human dopamine receptor subtypes using 11C-SCH 23390 and 11C-raclopride. Psychopharmacology (Berl) 1987; 92: 278-84
42. Farde L, Wiesel FA, Nordstrom AL, et al. D1- and D2-dopamine receptor occupancy during treatment with conventional and atypical neuroleptics. Psychopharmacology (Berl) 1989; 99: S28-31
43. Farde L. Selective D1- and D2-dopamine receptor blockade both induces akathisia in humans: a PET study with [11C]-SCH 23390 and [11C]raclopride. Psychopharmacology (Berl) 1992; 107: 23-9
44. Farde L, Nordstrom AL, Wiesel FA, et al. Positron emission tomographic analysis of central D1 and D2 dopamine receptor occupancy in patients treated with classical neuroleptics and clozapine: relation to extrapyramidal side effects. Arch Gen Psychiatry 1992; 49: 538-44
45. McQuade RD, Duffy RA, Coffin VL, et al. In vivo binding of SCH 39166: a D-1 selective antagonist. J Pharmacol Exp Ther 1991; 257: 42-9
46. Wagner HN, Burns HD, Dannals RF, et al. Imaging dopamine receptors in the human brain by positron tomography. Science 1983; 221: 1264-6
47. Maziere B, Loc'h C, Hantraye P, et al. 76Br-bromospiroperidol: a new tool for quantitative in-vivo imaging of neuroleptic receptors. Life Sci 1984; 35: 1349-56
48. Maziere B, Loc'h C, Stulzaft O, et al. [76Br]Bromolisuride: a new tool for quantitative in vivo imaging of D-2 dopamine receptors. Eur J Pharmacol 1986; 127: 239-47
49. Hantraye P, Brownell AL, Elmaleh D, et al. Dopamine fiber detection by 11C-CFT and PET in a primate model of Parkinsonism. Neuroreport 1992; 3: 265-8
50. Fischman AJ, Bonab AA, Babich JW, et al. [11C,127I]Altropane: a highly selective ligand for PET imaging of dopamine transporter sites. Synapse 2001; 39: 332-42
51. Blin J, Sette G, Fiorelli M, et al. A method for the in vivo investigation of the serotonergic 5-HT2 receptors in the human cerebral cortex using positron emission tomography and 18F-labeled setoperone. J Neurochem 1990; 54: 1744-54
52. Wong DF, Lever JR, Hartig PR, et al. Localization of serotonin 5-HT2 receptors in living human brain by positron emission tomography using N1-([11C]-methyl)-2-Br-LSD. Synapse 1987; 1: 393-8
53. Parsey RV, Slifstein M, Hwang DR, et al. J Cereb Blood Flow Metab 2000; 20: 1111-33
54. Maziere M, Hantraye P, Kaijima M, et al. Visualization by positron emission tomography of the apparent regional heterogeneity of central type benzodiazepine receptors in the brain of living baboons. Life Sci 1985; 36: 1609-16
55. Charbonneau P, Syrota A, Crouzel C, et al. Peripheral-type benzodiazepine receptors in the living heart characterized by positron emission tomography. Circulation 1986; 73: 476-83
56. Frost JJ, Mayberg HS, Fisher RS, et al. Mu-receptors measured by positron emission tomography are increased in temporal lobe epilepsy. Ann Neurol 1988; 23: 231-7
57. Jones AK, Luthra SK, Maziere B, et al. Regional cerebral opioid receptor studies with [11C]diprenorphine in normal volunteers. J Neurosci Methods 1988; 23: 121-9
58. Pert CB, Danks JA, Channing MA, et al. 3-[18F]Acetylcyclofoxy: a useful probe for the visualization of opiate receptors in living animals. FEBS Lett 1984; 177: 281-6
59. Syrota A, Paillotin G, Davy JM, et al. Kinetics of in vivo binding of antagonist to muscarinic cholinergic receptor in the human heart studied by positron emission tomography. Life Sci 1984; 35: 937-45
60. Dannals RF, Langstrom B, Ravert HT, et al. Synthesis of radiotracers for studying muscarinic cholinergic receptors in the living human brain using positron emission tomography: [11C]dexetimide and [11C]levetimide. Int J Rad Appl Instrum [A] 1988; 39: 291-5
61. Frey KA, Koeppe RA, Mulholland GK, et al. Muscarinic receptor imaging in human brain using [C-11] scopolamine and positron emission tomography [abstract]. J Nucl Med 1988; 29: 808
62. Dewey SL, MacGregor RR, Brodie JD, et al. Mapping muscarinic receptors in human and baboon brain using [N-11C-methyl]-benztropine. Synapse 1990; 5: 213-23
63. Syrota A. In vivo investigation of myocardial perfusion, metabolism and receptors by positron emission tomography. Int J Microcirc Clin Exp 1989; 8: 411-22
64. Frey KA, Hichwa RD, Ehrenkaufer RL, et al. Quantitative in vivo receptor binding III: tracer kinetic modeling of muscarinic cholinergic receptor binding. Proc Natl Acad Sci U S A 1985; 82: 6711-5
65. Wong DF, Gjedde A, Wagner HN, et al. Quantification of neuroreceptors in the living human brain: II. Inhibition studies of receptor density and affinity. J Cereb Blood Flow Metab 1986; 6: 147-53
66. Farde L, Eriksson L, Blomquist G, et al. Kinetic analysis of central [11C]raclopride binding to D2-dopamine receptors studied by PET: a comparison to the equilibrium analysis. J Cereb Blood Flow Metab 1989; 9: 696-708
67. Delforge J, Loch C, Hantraye P, et al. Kinetic analysis of central [76Br]bromolisuride binding to dopamine D2 receptors studied by PET. J Cereb Blood Flow Metab 1991; 11: 914-25
68. Morris ED, Alpert NM, Fischman AJ. Comparison of two compartmental models for describing receptor ligand kinetics and receptor availability in multiple injection PET studies. J Cereb Blood Flow Metab 1996; 16: 841-53
69. Huang SC, Bahn MM, Barrio JR, et al. A double-injection technique for in vivo measurement of dopamine D2-receptor density in monkeys with 3-(2′-[18F]fluoroethyl)spiperone and

dynamic positron emission tomography. J Cereb Blood Flow Metab 1989; 9: 850-8
70. Farde L, Hall H, Ehrin E, et al. Quantitative analysis of D2 dopamine receptor binding in the living human brain by PET. Science 1986; 231: 258-61
71. Huang SC, Barrio JR, Phelps ME. Neuroreceptor assay with positron emission tomography: equilibrium versus dynamic approaches. J Cereb Blood Flow Metab 1986; 6: 515-21
72. Farde L, Hall H, Ehrin E, et al. Quantitative analysis of D2 dopamine receptor binding in the living human brain by PET. Science 1986; 231: 258-61
73. Mintun MA, Raichle ME, Kilbourne MR, et al. A quantitative model for the in vivo assessment of drug binding sites with positron emission tomography. Ann Neurol 1984; 15: 217-27
74. Fischman AJ, Bonab AA, Babich JW, et al. Positron emission tomographic analysis of central 5HT2 receptor occupancy in healthy volunteers treated with the novel antipsychotic agent, ziprasidone. J Pharmacol Exp Ther 1996; 279: 939-47
75. Petit-Taboue MC, Landeau B, Osmont A, et al. Estimation of neocortical serotonin-2-receptor binding potential by single dose 18F-setoperone kinetic PET data analysis. J Nucl Med 1996; 37: 95-104
76. Christian BT, Livni E, Babich JW, et al. Evaluation of cerebral pharmacokinetics of the novel antidepressant drug, BMS-181101, by positron emission tomography. J Pharmacol Exp Ther 1996; 279: 325-31
77. Patlak CS, Blasberg RG, Fensternmacher JD. Graphical evaluation of blood-to-brain transfer constants in multiple-time uptake data. J Cereb Blood Flow Metab 1983; 3: 1-7
78. Logan J, Fowler JS, Volkow ND, et al. Graphical analysis of reversible radioligand binding from time-activity measurements applied to [N-11C-methyl]-(–)-cocaine PET studies in human subjects. J Cereb Blood Flow Metab 1990; 10: 740-7
79. Fukumoto M, Yoshida D, Hayase N, et al. Scintigraphic prediction of resistance to radiation and chemotherapy in patients with lung carcinoma: technetium 99m-tetrofosmin and thallium-201 dual single photon emission computed tomography study. Cancer 1999; 86: 1470-9
80. Malison RT, Best SE, Wallace EA, et al. Euphorigenic doses of cocaine reduce [123I] beta-CIT SPECT measures of dopamine transporter availability in human cocaine addicts. Psychopharmacology (Berl) 1995; 122: 358-62
81. Malison RT, McCance E, Carpenter LL, et al. [123I] beta-CIT SPECT imaging of dopamine transporter availability after mazindol administration in human cocaine addicts. Psychopharmacology (Berl) 1998; 137: 321-5
82. Christensen JD, Yurgelun-Todd DA, Babb SM, et al. Measurement of human brain dexfenfluramine concentration by 19F magnetic resonance spectroscopy. Brain Res 1999; 834: 1-5
83. Budinger TF. Emerging nuclear magnetic resonance techniques: health and safety. Ann N Y Acad Sci 1992; 649: 1-18
84. Wolf W, Presant CA, Waluch V. 19F-MRS studies of fluorinated drugs in humans. Adv Drug Deliv Rev 2000; 41: 55-74
85. Wolf W, Waluch V, Presant CA. Non-invasive 19F-MRS of 5-fluorouracil in pharmacokinetic and pharmacodynamic studies. NMR Biomed 1998; 11: 380-7
86. Belleman ME, Haberkorn U, Gerlach L, et al. Imaging of the biodistribution and metabolism of the antineoplastic agent gemcitabine in tumor bearing rats [abstract]. Proc Int Soc Magn Res Med 1999; 7: 1353
87. Workman P, Maxwell RJ, Griffiths JR. Non-invasive MRS in new anticancer drug development. NMR Biomed 1992; 5: 270-2
88. Aboagye EO, Maxwell RJ, Kelson AB, et al. Preclinical evaluation of the fluorinated 2-nitroimidazole N-(2- hydroxy-3,3,3-trifluoropropyl)-2-(2-nitro-1-imidazolyl) acetamide (SR-4554) as a probe for the measurement of tumor hypoxia. Cancer Res 1997; 57: 3314-8
89. He Q, Bhujwalla ZM, Maxwell RJ, et al. Proton NMR observation of the antineoplastic agent iproplatin in vivo by selective multiple quantum coherence transfer (Sel-MQC). Magn Reson Med 1995; 33: 414-6
90. Rodrigues LM, Maxwell RJ, McSheehy PM, et al. In vivo detection of ifosfamide by 31P-MRS in rat tumours: increased uptake and cytotoxicity induced by carbogen breathing in GH3 prolactinomas. Br J Cancer 1997; 75: 62-8
91. Artemov D, Bhujwalla ZM, Maxwell RJ, et al. Pharmacokinetics of the 13C labeled anticancer agent temozolomide detected in vivo by selective cross-polarization transfer. Magn Reson Med 1995; 34: 338-42
92. Becker M, Port RE, Zabel HJ, et al. Monitoring local disposition kinetics of carboplatin in vivo after subcutaneous injection in rats by means of 195Pt NMR. J Magn Reson 1998; 133: 115-22
93. Aboagye EO, Dillehay LE, Bhujwalla ZM, et al. Hypoxic cell cytotoxin tirapazamine induces acute changes in tumor energy metabolism and pH: a 31P magnetic resonance spectroscopy study. Radiat Oncol Investig 1998; 6: 249-54
94. Griffiths JR Glickson JD. Monitoring pharmacokinetics of anticancer drugs: non-invasive investigation using magnetic resonance spectroscopy. Adv Drug Deliv Rev 2000; 41: 75-89
95. Jynge P, Skjetne T, Gribbestad I, et al. In vivo tissue pharmacokinetics by fluorine magnetic resonance spectroscopy: a study of liver and muscle disposition of fleroxacin in humans. Clin Pharmacol Ther 1990; 48 (5): 481-9
96. Renshaw PF, Wicklund S. In vivo measurement of lithium in humans by nuclear magnetic resonance spectroscopy. Biol Psychiatry 1988; 23: 465-75
97. Gonzalez RG, Guimaraes AR, Sachs GS, et al. Measurement of human brain lithium in vivo by MR spectroscopy. AJNR Am J Neuroradiol 1993; 14: 1027-37
98. Renshaw PF, Guimaraes AR, Fava M, et al. Accumulation of fluoxetine and norfluoxetine in human brain during therapeutic administration. Am J Psychiatry 1992; 149: 1592-4
99. Henry ME, Moore CM, Kaufman MJ, et al. Brain kinetics of paroxetine and fluoxetine on the third day of placebo substitution: a fluorine MRS study. Am J Psychiatry 2000; 157: 1506-8

Correspondence and offprints: Dr *Alan J. Fischman*, Division of Nuclear Medicine, Massachusetts General Hospital, 32 Fruit Street, Boston, MA 02114, USA.